Journal of Materials Chemistry A

ROYAL SOCIETY OF CHEMISTRY

PAPER

View Article Online
View Journal

Cite this: DOI: 10.1039/d1ta08900e

High-performance anthraquinone with potentially low cost for aqueous redox flow batteries†

Min Wu, [a] Meisam Bahari, [a] Eric M. Fell, [a] Roy G. Gordon *[b] and Michael J. Aziz *[a]

Electrolyte cost and long-term durability are the two most challenging obstacles to the practical utilization of redox-active organics in aqueous redox flow batteries. Starting from potentially inexpensive 1,8-dihydroxyanthraquinone (1,8-DHAQ), we developed a one-pot, green, and scalable approach to synthesize a highly water-soluble and potentially low-cost anthraquinone 1,8-dihydroxy-2,7-dicarboxymethyl-9,10-anthraquinone (DCDHAQ). The demonstrated volumetric capacity of DCDHAQ in 1 M KOH is 40.2 A h L^{-1}, which is around 70 times higher than that of its precursor 1,8-DHAQ (0.567 A h L^{-1}) at pH 14. The introduction of $-CH_2CO_2^-$ as solubilizing groups suppressed the disproportionation reaction of reduced anthraquinone both thermodynamically and kinetically. Consequently, the cycling stability of anthraquinone was improved significantly compared to that of the precursor. Pairing a negolyte comprising 0.75 M DCDHAQ with a posolyte comprising 0.3 M ferrocyanide at pH 14, we demonstrated a cell with an open-circuit voltage of 1.1 V and a low capacity fade rate of 0.03% per day. The synthetic method of attaching $-CH_2CO_2^-$ as solubilizing groups is likely applicable to other anthraquinone derivatives and other aromatic organics as an inexpensive approach to performance enhancement in energy applications.

Received 15th October 2021
Accepted 16th November 2021

DOI: 10.1039/d1ta08900e

rsc.li/materials-a

Bulk electrical energy storage technologies have attracted great attention because of their capability to address the intrinsic intermittency of renewable energy sources such as solar and wind electricity.[1–3] Aqueous redox-flow batteries are particularly attractive for grid-scale energy storage owing to their flexible architecture, long cycle life, and good safety features.[3] Aqueous vanadium RFBs are the most commonly studied and adopted system, but their widespread application is hindered by the availability and the fluctuating price of vanadium.[2–4] In contrast, redox-active organics comprising earth-abundant elements such as C, H, O, and N are potentially inexpensive alternatives to vanadium.[5–7] Redox-active organics based on quinone,[8–20] viologen,[21–29] phenazine,[30–33] alloxazine,[34] and (2,2,6,6-tetramethylpiperidin-1-yl)oxyl[21,22,30,35–38] derivatives have been studied for aqueous redox flow batteries. However, only a few anthraquinone,[13,18,19] phenazine,[33] and viologen[24,26,27,29] derivatives have demonstrated very good long-term stability; others tend to have poor chemical stability. Viologens are vulnerable to attack by both protons and hydroxide, making their practical implementation difficult, as a small amount of a side reaction, *e.g.* with air leaking into the system, can lead to a large deviation from neutral pH.[24,29] Recently, phenazine derivatives have also been reported to be extremely stable; however, they suffer from high synthetic cost because expensive phenazine precursors, precious metal catalysts, and ligands are used for the synthesis.[33] All of the extremely stable anthraquinones reported to date, such as 2,6-DBEAQ,[13] 2,6-DPPEAQ,[18] DPivOHAQ,[19,20] and DBAQ,[19,20] also suffer from high chemical cost issues due to a multi-step synthesis or expensive precursors. Developing inexpensive, stable, and soluble redox-active organics remains crucial for the practical implementation of aqueous organic redox flow batteries (AORFBs).

Here, we report a potentially low-cost and highly soluble anthraquinone negolyte with good cycling stability. The anthraquinone 1,8-dihydroxy-2,7-dicarboxymethyl-9,10-anthraquinone (DCDHAQ) was synthesized from the relatively inexpensive precursor 1,8-dihydroxyanthraquinone (1,8-DHAQ) with a one-pot, green synthesis method with water as the solvent. The solubility of DCDHAQ at pH 14 is 1.3 M, which is almost two orders of magnitude higher that of its precursor 1,8-DHAQ (<0.02 M). The redox potential of DCDHAQ in 1 M KOH is −0.56 V *vs.* SHE; pairing with ferrocyanide, it enables a full cell voltage of 1.1 V. With this simple $-CH_2CO_2^-$ functionalization, the average capacity fade rate decreases from 0.85% per day for

[a]*John A. Paulson School of Engineering and Applied Sciences, Harvard University, Pierce Hall 204a, 29 Oxford Street, Cambridge, Massachusetts 02138, USA. E-mail: maziz@harvard.edu*

[b]*Department of Chemistry and Chemical Biology, Harvard University, 12 Oxford Street, Cambridge, Massachusetts 02138, USA. E-mail: gordon@chemistry.harvard.edu*

† Electronic supplementary information (ESI) available: Fig. S1–S10; Tables S1 and S2†; and detailed descriptions on the DCDHAQ and 1,4-CDHAQ synthesis, estimation of electrolyte cost, discussion of the relationship between state of charge, cut-off voltage and cell current. See DOI: 10.1039/d1ta08900e

1,8-DHAQ to as low as 0.03% per day for DCDHAQ. Moreover, the cost at mass-production scale is estimated to be approximately \$6–8 kg^{-1} (~\$40–50 kA h^{-1}), depending on synthetic route, potentially leading to a competitive flow battery chemistry. The inexpensive functionalization raises aqueous solubility, decreases molecular crossover rates, and greatly increases the cycling stability of anthraquinones, providing guidance for the rational design of redox-active organics for low cost and ultra-stable cycling performance.

DCDHAQ was synthesized *via* a one-pot, green synthesis method with an inexpensive precursor 1,8-DHAQ and finished in around 4 hours. As shown in Scheme 1, 1,8-DHAQ was reduced by sodium dithionite. Subsequently, the side-chain precursor, glyoxylic acid, was added to the solution, where the coupling reaction happened at room temperature to form 2,7-di-hydroxyacetic acid-1,8,9,10-tetrahydroxy-anthracene (DHATHAc). DHATHAc was further reduced with sodium dithionite and then air oxidized to form DCDHAQ.

Fig. 1a compares the aqueous solubility of 1,8-DHAQ and DCDHAQ. 1,8-DHAQ has a solubility of less than 0.02 M at pH 14, whereas DCDHAQ has a solubility of 1.3 M at pH 14, corresponding to a volumetric capacity of 70 A h L^{-1}. Thus, the volumetric capacity of anthraquinone increased by more than one order of magnitude with a simple chemical functionalization. The cyclic voltammograms (CV) of 1,8-DHAQ, DCDHAQ, and potassium ferrocyanide are shown in Fig. 1b. The redox potential of DCDHAQ at pH 14 is −0.56 V *vs.* SHE, which is 20 mV more positive than that of 1,8-DHAQ. The increased redox potential of anthraquinone is known to suppress the disproportionation side reaction of reduced anthraquinone thermodynamically,[39] thereby greatly increasing the cell cycling stability while slightly decreasing the cell voltage. Additionally, DCDHAQ has two additional negative charges compared to 1,8-DHAQ, which decrease the molecular crossover rate; the Coulomb repulsion also suppresses the rate of the disproportionation side reaction, thereby increasing the cell lifetime.[39,40] Pairing a DCDHAQ negolyte with a potassium ferri/ferrocyanide posolyte at pH 14 yields an equilibrium cell potential of approximately 1.06 V (Fig. 1b). The Pourbaix diagram of DCDHAQ redox is shown in Fig. 1c. Unlike most anthraquinones, which exhibit a constant redox potential for pH exceeding ~12, the redox potential of DCDHAQ continues to decrease as pH increases up to 14. Such behavior is also observed in 1,8-dihydroxyanthraquinone.[12] The addition of 1,8-dihydroxy-groups adds two additional pK_as to the reduced anthraquinone, thereby increasing the final pK_a of reduced anthraquinone from 12 to beyond 14. As the posolyte redox potential is pH-independent, a higher cell pH affords a higher full-cell voltage. The electrochemical properties of DCDHAQ were determined by rotating disk electrode (RDE) measurement as shown in Fig. 1d. The diffusion coefficient of DCDHAQ was calculated by the Levich equation:

$$i_L = 0.620nFAD^{\frac{2}{3}}\omega^{\frac{1}{2}}\nu^{-\frac{1}{6}}C \quad (1)$$

where i_L is the limiting current (mA) from the RDE test, n is the number of electrons transferred in the redox reaction, F is Faraday's constant (C mol^{-1}), A is the electrode area (cm^2), D is the diffusion coefficient (cm^2 s^{-1}), ω is the angular rotation rate of the electrode (rad s^{-1}), ν is the kinematic viscosity (cm^2 s^{-1}), and C is the analyte concentration (mol L^{-1}). Based on the slope of the linear i_L *vs.* $\omega^{1/2}$ curve in Fig. S3a,† D is 1.7×10^{-6} cm^2 s^{-1}, which is similar to values reported for other redox organics in aqueous condition.[41] The charge transfer coefficient was determined to be 0.54 based on the Tafel equation, and the electron transfer rate constant was determined to be 7.4×10^{-4} cm s^{-1}. The kinetic current was determined at different overpotentials by the Koutecký–Levich plot as shown in Fig. S4b.†

Capacity fade rate measurements with long-lived redox-active species are difficult because very low fade rates can be obscured by a capacity measurement artifact caused by a temporal variation in the cell resistance, *e.g.* from temperature drifts or membrane aging. To understand how to minimize the sensitivity of measurements of apparent capacity, *i.e.* the accessible state of charge (SOC) range, to such artifacts, we performed a numerical simulation of SOC with effective Nernstian voltage $E_{cell} - E^{0'}_{cell} - ir(i)$ for an anthraquinone capacity-limited or a capacity-balanced cell. Here E_{cell} is the potential applied to the cell, SOC is the fraction of all anthraquinones that is reduced, $E^{0'}_{cell}$ is the formal redox potential difference between posolyte and negolyte when each is 50% reduced, $ir(i)$ is the overall cell overpotential including ohmic overpotential, mass transport overpotential, and activation overpotential. And $r(i)$ is the effective, potentially nonlinear area-specific resistance accounting for all overpotentials. Thus $E_{cell} - E^{0'}_{cell} - ir(i)$ is an effective Nernstian voltage arising only from the relative concentrations of all the species in the two electrolytes. It should be noted that the simulation applies to both charge/discharge processes; in the charge process, i takes a positive value, while in the discharge process, i takes a negative value. With the assumptions that the anthraquinone composing the negolyte undergoes a two-electron redox process with both electron reduction potentials very close together, the ferrocyanide composing the posolyte undergoes a one-electron redox process, no irreversible electrochemical reactions are present, the activity coefficients are concentration-independent,

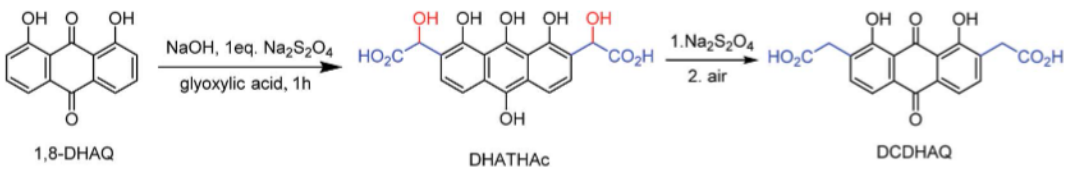

Scheme 1 Synthetic route for DCDHAQ.

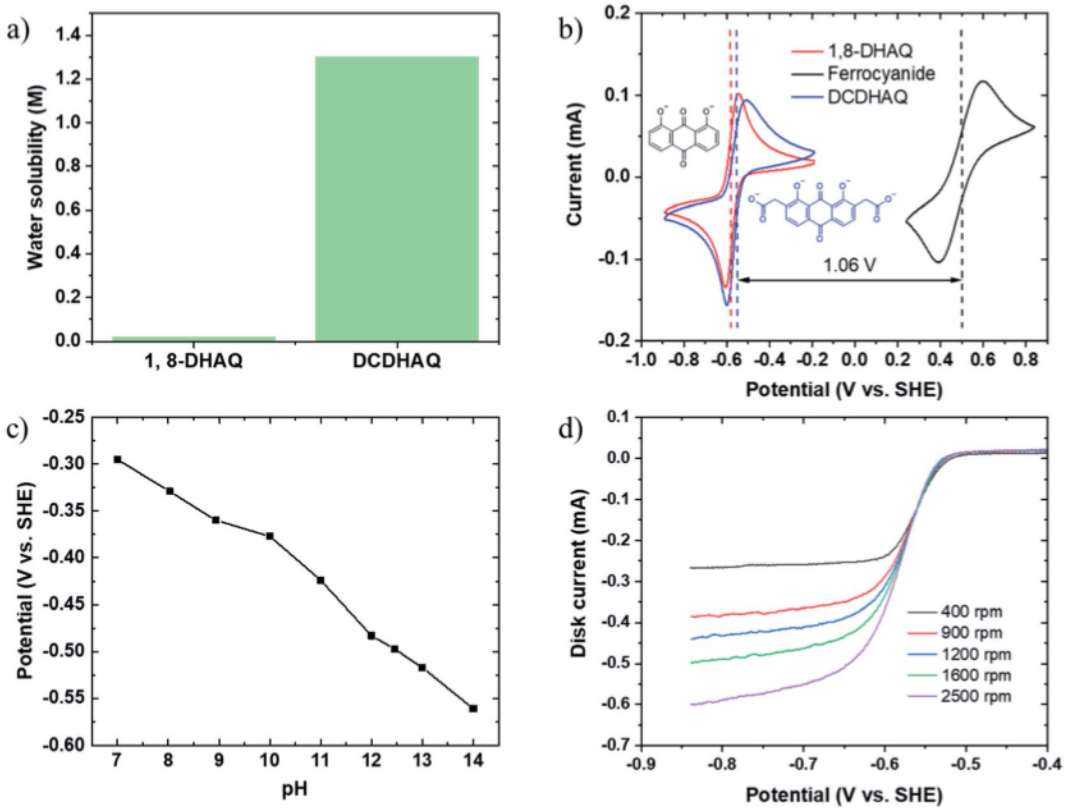

Fig. 1 (a) Solubility comparison for 1,8-DHAQ and DCDHAQ in 1 M KOH; (b) cyclic voltammograms of 5 mM 1,8-DHAQ, 5 mM DCDHAQ and 10 mM potassium ferrocyanide at pH 14 with a scan rate of 100 mV s^{-1}; (c) Pourbaix diagram of DCDHAQ redox process; (d) linear sweep voltammograms of 5 mM DCDHAQ in 1 M KOH on a rotating disk electrode at rotation rates between 400 and 2500 rpm.

and there is no complex formation among the species, the Nernst equation yields.

$$E_{\text{cell}} = E_{\text{cell}}^{0'} + ir(i) + \frac{RT}{2F}\ln\left(\frac{\text{SOC}}{1-\text{SOC}} \times \left(\frac{q+\text{SOC}}{p-\text{SOC}}\right)^2\right) \quad (2)$$

where R is the universal gas constant; T is the absolute temperature; F is Faraday's constant; and p and q represent the initial charge capacity ratio of ferrocyanide to total anthraquinone (oxidized plus reduced) and of ferricyanide to total anthraquinone, respectively (see ESI† for calculation details). The relationship between effective Nernstian voltage $E_{\text{cell}} - E_{\text{cell}}^{0'} - ir(i)$ and the SOC is plotted in Fig. 2a. It is clear that, to achieve an essentially full SOC, the magnitude of $E_{\text{cell}} - E_{\text{cell}}^{0'} - ir(i)$ should be 0.2 V or above, especially for a capacity balanced cell ($p = 1, q = 0$). Therefore, charging of the cell should be continued until the cell voltage is at least 0.2 V higher than $E_{\text{cell}}^{0'}$ for a two-electron redox molecule. Fig. 2b compares the dependence of $E_{\text{cell}} - E_{\text{cell}}^{0'} - ir(i)$ on SOC for a single-electron process in the posolyte and either a single-electron process or a two-electron process in the negolyte, suggesting that, other things being equal, accessing the same SOC requires charging to a higher cell voltage for a single-electron molecule than for a two-electron molecule.

A common method of investigating charge capacity and its fade rate is to charge the cell to a certain voltage (either potentiostatically or galvanostatically with a cutoff voltage), and then to hold at that voltage until the current density decays to a fixed cutoff value before switching polarity – and likewise for discharging. To investigate the relationship between maximum accessible SOC and cut-off current density, we present Fig. 2c, in which $r(i)$ is the effective area-specific resistance (potentially non-constant) accounting for all overpotentials over the entire SOC range. At intermediate SOC the activation overpotential has been shown to be ohmic for species with fast kinetics and the mass transport overpotential has been shown to be ohmic for reactant utilization (the fraction of reactant converted by the device in a single pass, which is proportional to the current divided by the product of reactant concentration and flow rate) up to about 40%.[42,43] It is apparent from Fig. 2c that, for current densities of tens of mA cm^{-2}, a small change in cell resistance, *e.g.* through aging or temperature drifts, leads to a significant change in maximum accessible SOC, leading to large fluctuations in apparent cell capacity and the inability to evaluate low capacity fade rates. For a cell with a non-ohmic mass transport overpotential, which may occur when the charging approaches the high-SOC limit where the concentration of available reactant becomes quite small and the utilization may become quite high, the mass transport overpotential increases superlinearly with current density.[43] The net effect of this nonlinear behavior is a move to the right along the curve for the current density under consideration. In other words, the assumption of ohmic

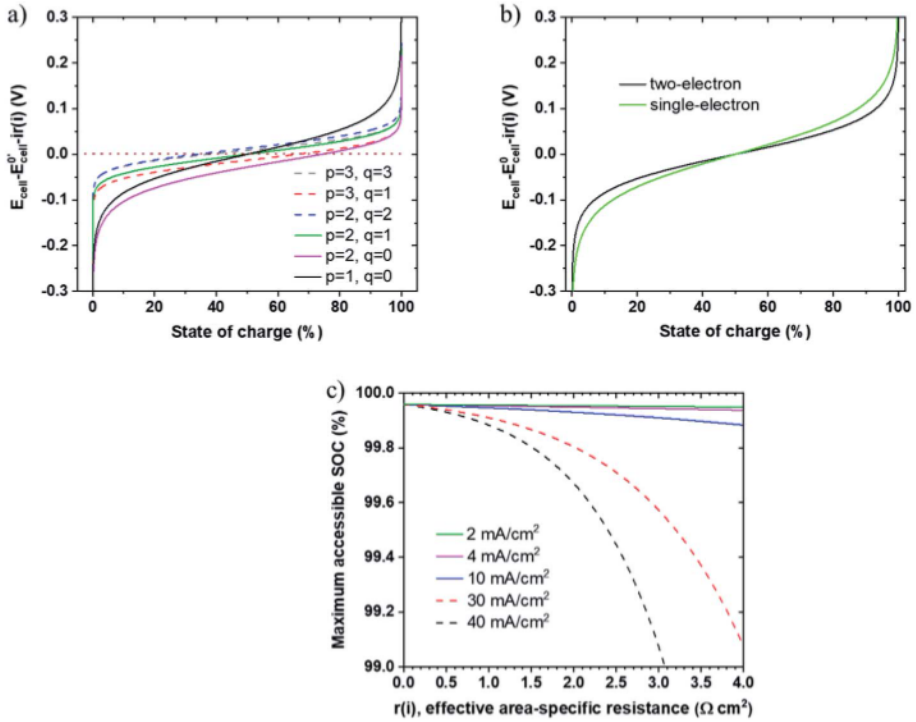

Fig. 2 Simulations for a cell with a capacity-limiting negolyte and a posolyte comprising one-electron redox molecules. (a) Calculated effective Nernstian voltage *vs.* SOC for negolyte comprising two-electron redox molecules of different electrolyte compositions; (b) calculated effective Nernstian voltage as a function of SOC for a capacity balanced cell ($p = 1$, $q = 0$) with negolyte undergoing a two-electron reaction or a single-electron reaction; (c) maximum accessible SOC *vs.* cell resistance for various cut-off current densities when $E_{cell} - E^{0'}_{cell} - ir(i)$ for a capacity-balanced cell ($p = 1$, $q = 0$) with negolyte comprising two-electron redox molecules.

behavior in Fig. 2c means that the curves represent an upper limit to the maximum accessible SOC. We conclude that, in order to measure stable high SOC values not subject to artifacts from drifting cell resistance, a potential hold until the current density drops to a small cut-off value is needed, as shown experimentally by Goulet and Aziz.[44] The simulation presented here serves as a guide for selecting numerical values of cycling voltage limits and cut-off current density for an accurate evaluation of discharge capacity and of slow capacity fade rates in redox flow batteries.

Polarization experiments of a 0.75 M DCDHAQ/ferrocyanide full cell at pH 14 were performed at various states of charge. The electrolytes comprised 5 mL of 0.75 M DCDHAQ (negolyte) at pH 14 (0.75 M H_4DCDHAQ combined with 2 M KOH and 2 M NaOH) and 40 mL of 0.3 M potassium ferrocyanide, 0.3 M potassium ferricyanide (posolyte) and 2 M NaCl at pH 14 (1 M KOH) to ensure that the negolyte always remained the capacity limiting side during both charging and discharging. We used mixed cations in the posolyte to raise the ferrocyanide solubility. To reduce the osmotic imbalance, NaOH and KOH were used in the DCDHAQ negolyte and NaCl was introduced into the posolyte. The concentrations were chosen such that the cation concentrations were balanced at intermediate SOC. The cell was constructed from graphite flow plates and AvCarb carbon cloth electrodes, separated by a Nafion 212 membrane pretreated in 1 M KOH to avoid changing the pH of the electrolytes. The carbon electrode was untreated and used directly in all cell measurements, as commercial AvCarb carbon cloth is hydrophilic. To determine its initial capacity, the cell was first charged and discharged galvanostatically with a potential hold at 1.5 and 0.65 V, respectively, until the current density dropped to 2 mA cm^{-2}. Then, the cell was charged to different SOC to measure the open-circuit voltage (OCV). The OCV increases from 1.1 to 1.23 V as the SOC increases from 10% to ~90% (Fig. 3a). The OCV at 50% SOC is approximately 1.16 V. A peak galvanic power density of 0.16 W cm^{-2} was achieved at ~90% SOC (Fig. 3b). The power density may be increased by engineering improvements such as the incorporation of lower-resistance membranes.

Long-term galvanostatic cycling of the 0.2 M DCDHAQ/ferrocyanide cell was performed at 50 mA cm^{-2} with potential holds at 1.4 V for charging and 0.8 V for discharging until the current density dropped to 2 mA cm^{-2} (Fig. 3c). The electrolytes comprised 5 mL of 0.2 M DCDHAQ (negolyte) at pH 14 and 40 mL of 0.2 M potassium ferrocyanide + 0.02 M potassium ferricyanide (posolyte) at pH 14. The initial discharge capacity at full SOC was 10.67 A h L^{-1} (theoretical value 10.72 A h L^{-1}). After 2.1 days of full SOC range cycling, the capacity faded by 0.19%, corresponding to a temporal capacity fade rate of 0.09% per day or 0.0017% per cycle. We expect fade rates measured this way in full cells to provide upper limits on true molecular decomposition rates because of the possible contribution of molecular crossover. For the next 6.4 days, the cell continued to be charged galvanostatically to 90% SOC at 50 mA cm^{-2} and immediately

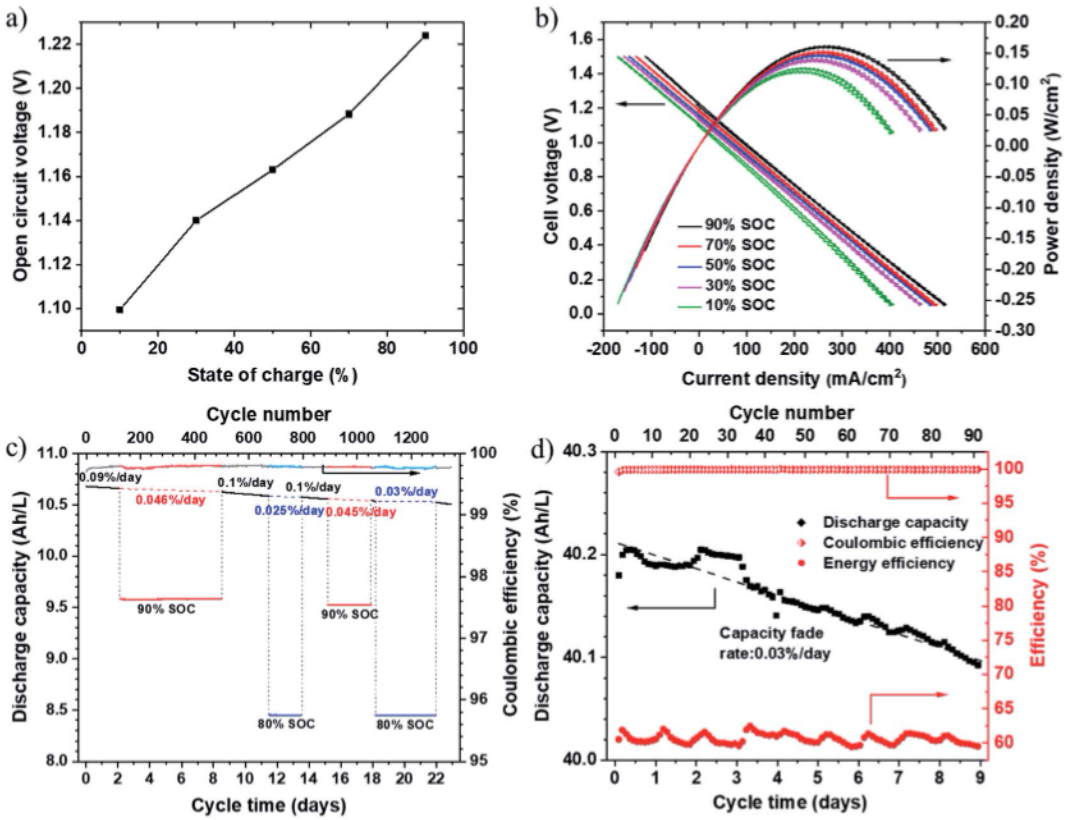

Fig. 3 (a) Open circuit voltage of 0.75 M DCDHAQ/0.3 M potassium ferrocyanide + 0.3 M potassium ferricyanide full cell at pH 14; (b) polarization measurements of the corresponding 0.75 M full cell at pH 14; (c) cell cycling of 5 mL 0.2 M DCDHAQ and 30 mL 0.2 M ferrocyanide + 0.02 M ferricyanide at pH 14; (d) discharge capacity, coulombic efficiency, and round-trip energy efficiency during cycling of 0.75 M DCDHAQ with 0.3 M potassium ferrocyanide and 0.3 M potassium ferricyanide full cell at pH 14.

discharged to 0.8 V at 50 mA cm^{-2} with a potential hold, until the current density dropped to 2 mA cm^{-2}. The cell was subsequently charged back to full SOC to evaluate the capacity fade rate during cycling when charging had been limited to 90% SOC. The capacity fade rate when charging was limited to 90% SOC was determined to be 0.046% per day or 0.00074% per cycle. Similarly, the average capacity fade rate when charging was limited to 80% SOC was around 0.03% per day. The increased cycling stability at lower charge-limiting SOC suggests that the capacity fade was due to the formation of electrochemically inactive anthrone, which is known to be suppressed by limiting charging during cycling.[39] Cycling was continued at different limiting SOCs (100%, 90%, 100%, 80%, 100%, 90%, 100%, 80%, 100%) for 23 days, and the discharge capacity was always determined immediately after fully charging the cell. The average capacity fade rate for the 23 days of cycling was 0.068% per day or 0.0011% per cycle with an average coulombic efficiency of 99.8%. As shown in Table S1,† which excludes results from molecules requiring multiple synthetic steps or expensive precursors, this stands out as the most stable cell performance to date with potentially low-cost redox-active organic molecules.

Long-term cycling of the 0.75 M DCDHAQ/ferrocyanide cell was performed at 40 mA cm^{-2} with potential holds at 1.5 V for charging and 0.65 V for discharging until the current density dropped to 2 mA cm^{-2} (Fig. 3d). The composition and volumes of the electrolytes are the same as those in the polarization experiment. It should be noted that the great excess of posolyte used here keeps the state of charge in the posolyte relatively invariant and prevents the posolyte from becoming capacity limiting, thereby enabling the accurate determination of the negolyte capacity fade rate. In practical deployment, such an excess is unnecessary. The wide voltage window and low cut-off current density applied here should access the full cell capacity, according to the simulation results presented in Fig. 2. When the cut-off voltage with respect to the measured OCV and the cut-off current density are appropriate as the simulations suggest, measurements of capacity and true capacity fade rate reflect losses from chemical decomposition, leakage, or crossover of active species from the capacity limiting side.[45] The initial volumetric capacity was 40.2 A h L^{-1}, which is equal to the theoretical capacity. The measured volumetric capacity is one of the highest capacities demonstrated experimentally for AORFBs.[14,17] The coulombic efficiency is above 99.9% over the whole cycling process. Although the round-trip energy efficiency exhibits large fluctuations in Fig. 3d due to daily temperature oscillations in the laboratory, the daily capacity fluctuation was much smaller; this highlights the importance of the potential-hold method to accurately evaluate the capacity fade rate. After 9 days of cycling, the volumetric capacity faded by 0.27%, which corresponded to a temporal capacity fade of 0.03% per

day, or 0.0029% per cycle, representing one of the most stable organics reported.[3] The DCDHAQ electrolytes before and after cycling were analyzed with ^{1}H NMR. As shown in Fig. S5,† no apparent chemical decomposition was observed, indicating the high chemical stability of DCDHAQ molecule.

For comparison, a 1,8-DHAQ/ferrocyanide full cell was cycled at pH 14. The negolyte consisted of 6 mL saturated 1,8-DHAQ at pH 14 (1 M KOH) and the posolyte consisted of 30 mL 0.1 M potassium ferrocyanide and 0.02 M potassium ferricyanide at pH 14 (1 M KOH). The membrane was Nafion 212, and the electrode was untreated AvCarb carbon electrodes, as in the DCDHAQ/ferrocyanide cell. The cell was cycled between 0.8–1.4 V with a potential hold until the current dropped to 2 mA cm^{-2}. The initial volumetric capacity for the saturated 1,8-DHAQ at pH 14 was 0.567 A h L^{-1} as shown in Fig. S6,† which is less than 2% of the demonstrated volumetric capacity in the DCDHAQ cell. The cell lost 2% of its capacity in the first half day, and then the capacity fade rate decayed to around 0.85% per day, which is much higher than that of DCDHAQ cell at 0.2 M (0.09% per day) and 0.75 M concentration (0.03% per day). Overall, the introduction of two –CH_2CO_2H groups not only increases the volumetric capacity but also greatly increases the anthraquinone lifetime.

When considering the potential for practical deployment, the electrolyte cost at a commercial scale is one of the most important factors but is also one of the most difficult to assess for a new composition of matter. The laboratory-scale cost of the precursor 1,8-DHAQ is low compared to that of its isomer 2,6-DHAQ, as shown in Table S2 (see Estimated cost of electrolytes in the ESI†). Given that DCDHAQ synthesis is a one-pot green method that uses water as the solvent and inexpensive glyoxylic acid as the chain precursor, its synthetic cost at a commercial scale should be low. Additionally, the reaction should also proceed with an electrochemical synthesis method such as that shown in Fig. S7,† which would avoid the use of sodium dithionite. As discussed in the ESI,† the mass-production cost of DCDHAQ is estimated to be approximately \$8–10.4 kg^{-1} by the chemical synthetic route reported here and between \$6–8 kg^{-1} by the electrochemical synthetic route.

To demonstrate the generality of the synthetic method of attaching glyoxylic acid groups, we attached a single –CH_2-COOH group to 1,4-DHAQ, forming 1,4-dihydroxy-2-carboxymethyl-9,10-anthraquinone (1,4-CDHAQ), as shown in Fig. 4. Compared to DCDHAQ, the mass-production cost of 1,4-CDHAQ may be lower because of the lower cost of 1,4-DHAQ (Table S2†) and the use of only half as much of the chain precursor as for DCDHAQ. 1,4-DHAQ is readily produced from phthalic anhydride and 4-chlorophenol; thus, it is the least expensive of the DHAQ family with a cost comparable to that of anthraquinone.[46] The solubility at pH 14 of 1,4-CDHAQ is 1.0 M, corresponding to a volumetric capacity of 53.6 A h L^{-1}, which is more than 10 times that of 1,4-DHAQ (Fig. S8†) and comparable to that of DCDHAQ. The redox potential of 1,4-CDHAQ is −0.56 V *vs.* SHE at pH 14, enabling it to form a 1.05 V full cell when paired with potassium ferrocyanide (Fig. 4b). Unfortunately, 1,4-CDHAQ appears, based on color changes in Fig. S9† and current decreases in CV results in Fig. S10,† to react

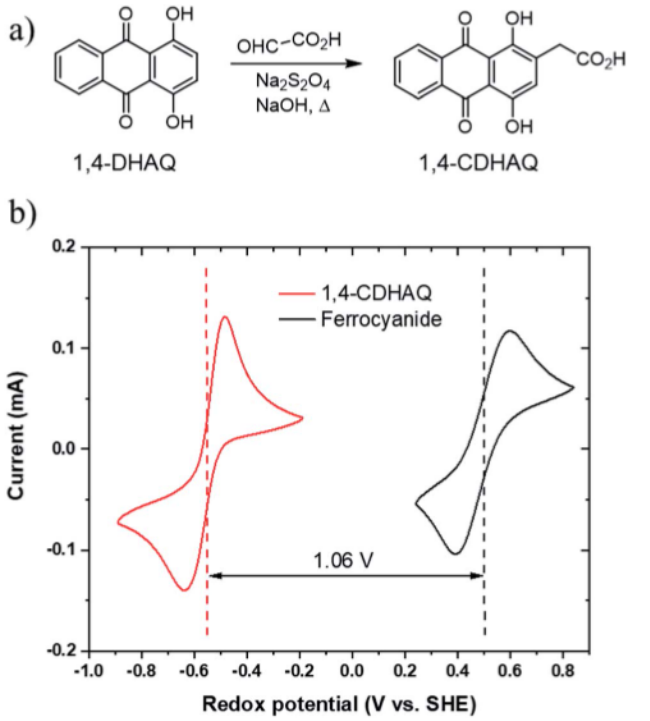

Fig. 4 (a) Synthetic route for 1,4-CDHAQ; (b) cyclic voltammograms of 5 mM 1,4-CDHAQ and 10 mM potassium ferrocyanide at pH 14 with a scan rate of 100 mV s^{-1}.

irreversibly with ferricyanide. The irreversible decomposition is tentatively attributed to the oxidation of 1,4-hydroxy groups in 1,4-CDHAQ by ferricyanide, followed by Michael addition. A similar decomposition mechanism has been observed in both alizarin and quinizarin derivatives at high oxidation potential.[47] Since the crossover of ferricyanide cannot be avoid in Nafion 212 membrane, thus cell-scale performance evaluation of 1,4-CDHAQ must await a membrane with a negligible ferricyanide crossover rate and not evaluated here.

We showed how simple molecular modification of a potentially inexpensive but poorly-performing aromatic precursor can improve the performance of redox-active organics in aqueous flow batteries. We demonstrated a high-performance AORFB with a highly soluble, stable, and potentially inexpensive anthraquinone in the negolyte. Because glyoxylic acid is known to react with phenol,[48] the potentially inexpensive synthetic method of attaching glyoxylate groups on aromatics might be readily extended to other anthraquinone derivatives and perhaps other aromatics, accelerating the development of redox-active organics for practical application. Finally, the simulated results relating SOC to cycling voltage limits and cut-off current density provide quantitative guidance for accurate evaluation of cell capacity and its fade rate.

Conflicts of interest

M. J. A. and M. B. have an ownership stake in Quino Energy, Inc., which may profit from the materials reported herein.

Acknowledgements

This research was supported by U.S. DOE award DE-AC05-76RL01830 through PNNL subcontract 535264 and Innovation Fund Denmark *via* the Grand Solutions project "ORBATS" file no. 7046-00018B. The authors thank Dr Eugene Beh, Dr Yan Jing, Martin Jin, Emily Kerr, Daniel Pollack, and Jinxu Gao for valuable discussions.

References

1 B. Dunn, H. Kamath and J.-M. Tarascon, Electrical Energy Storage for the Grid: A Battery of Choices, *Science*, 2011, **334**, 928–935.

2 G. L. Soloveichik, Flow Batteries: Current Status and Trends, *Chem. Rev.*, 2015, **115**(20), 11533–11558.

3 D. G. Kwabi, Y. Ji and M. J. Aziz, Electrolyte lifetime in aqueous organic redox flow batteries: A critical review, *Chem. Rev.*, 2020, **120**(14), 6467–6489.

4 R. M. Darling, K. G. Gallagher, J. A. Kowalski, S. Ha and F. R. Brushett, Pathways to low-cost electrochemical energy storage: a comparison of aqueous and nonaqueous flow batteries, *Energy Environ. Sci.*, 2014, **7**(11), 3459–3477.

5 X. L. Wei, W. X. Pan, W. T. Duan, A. Hollas, Z. Yang, B. Li, Z. M. Nie, J. Liu, D. Reed, W. Wang and V. Sprenkle, Materials and Systems for Organic Redox Flow Batteries: Status and Challenges, *ACS Energy Lett.*, 2017, **2**(9), 2187–2204.

6 J. A. Luo, B. Hu, M. W. Hu, Y. Zhao and T. L. Liu, Status and Prospects of Organic Redox Flow Batteries toward Sustainable Energy Storage, *ACS Energy Lett.*, 2019, **4**(9), 2220–2240.

7 F. R. Brushett, M. J. Aziz and K. E. Rodby, On lifetime and cost of redox-active organics for aqueous flow batteries, *ACS Energy Lett.*, 2020, **5**, 879–884.

8 B. T. Huskinson, M. P. Marshak, C. Suh, S. Er, M. R. Gerhardt, C. J. Galvin, X. Chen, A. Aspuru-Guzik, R. G. Gordon and M. J. Aziz, A metal-free organic-inorganic aqueous flow battery, *Nature*, 2014, **505**(7482), 195–198.

9 K. Lin, Q. Chen, M. R. Gerhardt, L. Tong, S. B. Kim, L. Eisenach, A. W. Valle, D. Hardee, R. G. Gordon, M. J. Aziz and M. P. Marshak, Alkaline quinone flow battery, *Science*, 2015, **349**(6255), 1529–1532.

10 M. R. Gerhardt, L. Tong, R. Gomez-Bombarelli, Q. Chen, M. P. Marshak, C. J. Galvin, A. Aspuru-Guzik, R. G. Gordon and M. J. Aziz, Anthraquinone Derivatives in Aqueous Flow Batteries, *Adv. Energy Mater.*, 2017, **7**(8), 1601488.

11 Z. Yang, L. Tong, D. P. Tabor, E. S. Beh, M. A. Goulet, D. De Porcellinis, A. Aspuru-Guzik, R. G. Gordon and M. J. Aziz, Alkaline Benzoquinone Aqueous Flow Battery for Large-Scale Storage of Electrical Energy, *Adv. Energy Mater.*, 2018, **8**(8), 1702056.

12 J. Y. Cao, M. Tao, H. P. Chen, J. Xu and Z. D. Chen, A highly reversible anthraquinone-based anolyte for alkaline aqueous redox flow batteries, *J. Power Sources*, 2018, **386**, 40–46.

13 D. G. Kwabi, K. Lin, Y. Ji, E. F. Kerr, M.-A. Goulet, D. De Porcellinis, D. P. Tabor, D. A. Pollack, A. Aspuru-Guzik, R. G. Gordon and M. J. Aziz, Alkaline quinone flow battery with long lifetime at pH 12, *Joule*, 2018, **2**(9), 1907–1908.

14 S. Jin, Y. Jing, D. G. Kwabi, Y. Ji, L. Tong, D. De Porcellinis, M. A. Goulet, D. A. Pollack, R. G. Gordon and M. J. Aziz, A water-miscible quinone flow battery with high volumetric capacity and energy density, *ACS Energy Lett.*, 2019, **4**(6), 1342–1348.

15 M. Park, E. S. Beh, E. M. Fell, Y. Jing, E. F. Kerr, D. De Porcellinis, M. A. Goulet, J. Ryu, A. A. Wong, R. G. Gordon, J. Cho and M. J. Aziz, A High Voltage Aqueous Zinc-Organic Hybrid Flow Battery, *Adv. Energy Mater.*, 2019, **9**(25), 1900694.

16 L. Tong, M.-A. Goulet, D. P. Tabor, E. F. Kerr, D. De Porcellinis, E. M. Fell, A. Aspuru-Guzik, R. G. Gordon and M. J. Aziz, Molecular Engineering of an Alkaline Naphthoquinone Flow Battery, *ACS Energy Lett.*, 2019, **4**(8), 1880–1887.

17 B. Hu, J. Luo, M. Hu, B. Yuan and T. L. Liu, A pH-Neutral, Metal-Free Aqueous Organic Redox Flow Battery Employing an Ammonium Anthraquinone Anolyte, *Angew. Chem., Int. Ed.*, 2019, **58**(46), 16629–16636.

18 Y. Ji, M. A. Goulet, D. A. Pollack, D. G. Kwabi, S. Jin, D. Porcellinis, E. F. Kerr, R. G. Gordon and M. J. Aziz, A Phosphonate-Functionalized Quinone Redox Flow Battery at Near-Neutral pH with Record Capacity Retention Rate, *Adv. Energy Mater.*, 2019, **9**(12), 1900039.

19 M. Wu, Y. Jing, A. A. Wong, E. M. Fell, S. Jin, Z. Tang, R. G. Gordon and M. J. Aziz, Extremely stable anthraquinone negolytes synthesized from common precursors, *Chem*, 2020, **6**, 11.

20 Y. Jing, M. Wu, A. A. Wong, E. M. Fell, S. Jin, D. A. Pollack, E. F. Kerr, R. G. Gordon and M. J. Aziz, In situ electrosynthesis of anthraquinone electrolytes in aqueous flow batteries, *Green Chem.*, 2020, **22**(18), 6084–6092.

21 T. B. Liu, X. L. Wei, Z. M. Nie, V. Sprenkle and W. Wang, A Total Organic Aqueous Redox Flow Battery Employing a Low Cost and Sustainable Methyl Viologen Anolyte and 4-HO-TEMPO Catholyte, *Adv. Energy Mater.*, 2015, **6**(3), 1501449.

22 T. Janoschka, S. Morgenstern, H. Hiller, C. Friebe, K. Wolkersdorfer, B. Haupler, M. D. Hager and U. S. Schubert, Synthesis and characterization of TEMPO- and viologen-polymers for water-based redox-flow batteries, *Polym. Chem.*, 2015, **6**(45), 7801–7811.

23 B. Hu, C. DeBruler, Z. Rhodes and T. L. Liu, Long-Cycling Aqueous Organic Redox Flow Battery (AORFB) toward Sustainable and Safe Energy Storage, *J. Am. Chem. Soc.*, 2017, **139**(3), 1207–1214.

24 E. S. Beh, D. De Porcellinis, R. L. Gracia, K. T. Xia, R. G. Gordon and M. J. Aziz, A Neutral pH Aqueous Organic-Organometallic Redox Flow Battery with Extremely High Capacity Retention, *ACS Energy Lett.*, 2017, **2**(3), 639–644.

25 J. Luo, B. Hu, C. Debruler and T. L. Liu, A pi-Conjugation Extended Viologen as a Two-Electron Storage Anolyte for Total Organic Aqueous Redox Flow Batteries, *Angew. Chem., Int. Ed.*, 2018, **57**(1), 231–235.

26 C. DeBruler, B. Hu, J. Moss, J. Luo and T. L. Liu, A Sulfonate-Functionalized Viologen Enabling Neutral Cation Exchange, Aqueous Organic Redox Flow Batteries toward Renewable Energy Storage, *ACS Energy Lett.*, 2018, **3**(3), 663–668.

27 W. Liu, Y. Liu, H. Zhang, C. Xie, L. Shi, Y. G. Zhou and X. Li, A highly stable neutral viologen/bromine aqueous flow battery with high energy and power density, *Chem. Commun.*, 2019, **55**(33), 4801–4804.

28 A. Ohira, T. Funaki, E. Ishida, J.-D. Kim and Y. Sato, Redox-Flow Battery Operating in Neutral and Acidic Environments with Multielectron-Transfer-Type Viologen Molecular Assembly, *ACS Appl. Energy Mater.*, 2020, **3**(5), 4377–4383.

29 S. Jin, E. M. Fell, L. Vina-Lopez, Y. Jing, P. W. Michalak, R. G. Gordon and M. J. Aziz, Near Neutral pH Redox Flow Battery with Low Permeability and Long-Lifetime Phosphonated Viologen Active Species, *Adv. Energy Mater.*, 2020, **10**(20), 2000100.

30 J. Winsberg, C. Stolze, S. Muench, F. Liedl, M. D. Hager and U. S. Schubert, TEMPO/Phenazine Combi-Molecule: A Redox-Active Material for Symmetric Aqueous Redox-Flow Batteries, *ACS Energy Lett.*, 2016, **1**(5), 976–980.

31 A. Hollas, X. L. Wei, V. Murugesan, Z. M. Nie, B. Li, D. Reed, J. Liu, V. Sprenkle and W. Wang, A biomimetic high-capacity phenazine-based anolyte for aqueous organic redox flow batteries, *Nat. Energy*, 2018, **3**(6), 508–514.

32 C. Wang, X. Li, B. Yu, Y. Wang, Z. Yang, H. Wang, H. Lin, J. Ma, G. Li and Z. Jin, Molecular Design of Fused-Ring Phenazine Derivatives for Long-Cycling Alkaline Redox Flow Batteries, *ACS Energy Lett.*, 2020, **5**(2), 411–417.

33 S. Pang, X. Wang, P. Wang and Y. Ji, Biomimetic Amino Acid Functionalized Phenazine Flow Batteries with Long Lifetime at Near-Neutral pH, *Angew. Chem., Int. Ed.*, 2021, **60**, 5289–5298.

34 K. Lin, R. Gomez-Bombarelli, E. S. Beh, L. Tong, Q. Chen, A. Valle, A. Aspuru-Guzik, M. J. Aziz and R. G. Gordon, A redox-flow battery with an alloxazine-based organic electrolyte, *Nat. Energy*, 2016, **1**(9), 16102.

35 J. Winsberg, T. Janoschka, S. Morgenstern, T. Hagemann, S. Muench, G. Hauffman, J. F. Gohy, M. D. Hager and U. S. Schubert, Poly(TEMPO)/Zinc Hybrid-Flow Battery: A Novel, "Green", High Voltage, and Safe Energy Storage System, *Adv. Mater.*, 2016, **28**(11), 2238–2243.

36 Z. Chang, D. Henkensmeier and R. Chen, One-Step Cationic Grafting of 4-Hydroxy-TEMPO and its Application in a Hybrid Redox Flow Battery with a Crosslinked PBI Membrane, *ChemSusChem*, 2017, **10**(16), 3193–3197.

37 J. Winsberg, C. Stolze, A. Schwenke, S. Muench, M. D. Hager and U. S. Schubert, Aqueous 2,2,6,6-Tetramethylpiperidine-N-oxyl Catholytes for a High-Capacity and High Current Density Oxygen-Insensitive Hybrid-Flow Battery, *ACS Energy Lett.*, 2017, **2**(2), 411–416.

38 Y. H. Liu, M. A. Goulet, L. C. Tong, Y. Z. Liu, Y. L. Ji, L. Wu, R. G. Gordon, M. J. Aziz, Z. J. Yang and T. W. Xu, A Long-Lifetime All-Organic Aqueous Flow Battery Utilizing TMAP-TEMPO Radical, *Chem*, 2019, **5**(7), 1861–1870.

39 M.-A. Goulet, L. Tong, D. A. Pollack, D. P. Tabor, S. A. Odom, A. Aspuru-Guzik, E. E. Kwan, R. G. Gordon and M. J. Aziz, Extending the lifetime of organic flow batteries *via* redox state management, *J. Am. Chem. Soc.*, 2019, **141**(20), 8014–8019.

40 B. Hu, Y. Tang, J. Luo, G. Grove, Y. Guo and T. L. Liu, Improved radical stability of viologen anolytes in aqueous organic redox flow batteries, *Chem. Commun.*, 2018, **54**(50), 6871–6874.

41 F. Gharagheizi, Determination of Diffusion Coefficient of Organic Compounds in Water Using a Simple Molecular-Based Method, *Ind. Eng. Chem. Res.*, 2012, **51**(6), 2797–2803.

42 Q. Chen, M. R. Gerhardt and M. J. Aziz, Dissection of the voltage losses of an acidic quinone redox flow battery, *J. Electrochem. Soc.*, 2017, **164**(6), A1126.

43 A. A. Wong and M. J. Aziz, Method for Comparing Porous Carbon Electrode Performance in Redox Flow Batteries, *J. Electrochem. Soc.*, 2020, **167**, 110542.

44 M. A. Goulet and M. J. Aziz, Flow battery molecular reactant stability determined by symmetric cell cycling methods, *J. Electrochem. Soc.*, 2018, **165**(7), A1466.

45 Q. Chen, L. Eisenach and M. J. Aziz, Cycling Analysis of a Quinone-Bromide Redox Flow Battery, *J. Electrochem. Soc.*, 2016, **163**(1), A5057–A5063.

46 H.-S. Bien, J. Stawitz and K. Wunderlich, Anthraquinone Dyes and Intermediates, in *Ullmann's Encyclopedia of Industrial Chemistry*, 2000.

47 L. Tong, Y. Jing, R. G. Gordon and M. J. Aziz, Symmetric All-Quinone Aqueous Battery, *ACS Appl. Energy Mater.*, 2019, **2**(6), 4016–4021.

48 G. Mattioda and Y. Christidis, Glyoxylic Acid, in *Ullmann's Encyclopedia of Industrial Chemistry*, 2000.

